Pergamon

Int. J. Heat Mass Transfer. Vol. 38, No. 12, pp. 2225–2238, 1995

0017-9310/95 $9.50+0.00

0017-9310(94)00333-5

Effects of variable viscosity and viscous dissipation on laminar convection heat transfer of a power law fluid in the entrance region of a semi-circular duct

S. GH. ETEMAD and A. S. MUJUMDAR†

Department of Chemical Engineering, McGill University, 3480 University Street, Montreal, Quebec, Canada H3A 2A7

(*Received* 7 *February* 1994 *and in final form* 19 *October* 1994)

Abstract—A numerical scheme based on Galerkin's finite element method was used to solve the three-dimensional governing equations for steady laminar simultaneously developing flow and heat transfer in a semi-circular duct. Two different boundary conditions, constant wall heat flux both axially and peripherally and constant wall temperature, were considered. The study was conducted for a purely viscous non-Newtonian fluid with different power law indices and Prandtl numbers. The effects of temperature dependent viscosity and viscous dissipation were examined and discussed.

INTRODUCTION

Internal fins and twisted-strips can be used as effective techniques for enhancing heat transfer in circular tubes. Such techniques find application in many compact heat exchangers and have motivated many research investigations. In the limiting case of a twisted strip, the strip is straight and thin and the tube is thus divided into two semi-circular ducts. The semi-circular duct is also the limiting case for internally finned tubes with full tapered fins. The presence of fin or strip changes the flow pattern and hence the pressure drop and heat transfer. It is therefore important to have a detailed knowledge of the fluid flow and heat transfer coefficients for semi-circular ducts.

Laminar flow heat transfer in circular and non-circular cross sectional ducts has been surveyed extensively by Shah and London [1] and Shah and Bhatti [2]. The hydrodynamically and thermally fully developed flow in semi-circular tubes with different apex angles (varying from 1 to 60°) was first analyzed by Eckert *et al.* [3] for constant heat flux boundary conditions. Sparrow and Haji-Sheikh [4] extended this work and obtained results for $0° \leqslant 2\varphi \leqslant 180°$. Hu [5] and Hu and Chang [6] solved the governing equations for steady fully developed laminar flow and heat transfer for internally finned tubes subjected to the $H2$ (constant heat flux both axially and peripherally) boundary conditions. When the number of fins is one, the duct is a semi-circular channel. Soliman *et al.* [7] numerically analyzed the laminar flow in the entrance region of circular sector ducts with apex angles from 11.25–90°. The Fourier transform technique was used by Lei and Trupp [8] to obtain results for fully developed steady laminar Newtonian flow, and [9] analyzed the fully developed flow and heat transfer for the $H1$ (constant wall heat flux axially and constant wall temperature peripherally) boundary condition and [10] for the $H2$ thermal boundary condition in circular sector ducts. Trupp and Lau [11] employed the finite difference technique for laminar heat transfer in circular sector ducts with isothermal walls for apex angles from 8 to 180°. Also Ben-Ali *et al.* [12] applied this numerical method to predict the heat and fluid flow behavior for different boundary conditions in annular sector and circular sector channels with apex angles from 5 to 350°.

The hydrodynamically developed but thermally developing case was investigated numerically using the finite difference method by Hong and Bergles [13] for $H1$, Manglik and Bergles [14] for T (constant wall temperature axially and peripherally) and Lei and Trupp [15] for $H1$ and $H2$ boundary conditions. The work of Lei and Trupp [15] covers results for apex angle from 20 to 360°. Prakash and Liu [16] reported local Nusselt numbers for simultaneously developing flow and heat transfer of circular sector ducts with apex angles of 45, 22.5 and 5°. They employed the control volume finite difference method to solve the parabolized governing equations.

Hsia and Chung [17] employed the finite difference approach to solve the hydrodynamically fully developed and thermally developing case for a power law fluid flowing through annular sector ducts under the $H1$ boundary condition, including viscous dissipation effects. Dasmahapatra and Hsia [18] experimentally studied the fluid flow and heat transfer of

†Author to whom correspondence should be addressed.

NOMENCLATURE

A	cross sectional area
B	dimensionless temperature–viscosity coefficient defined by equations (11) and (12)
B'	temperature–viscosity coefficient defined by equation (2)
Br	Brinkman number [$= k_0 u_e^{n+1}/K(T_e - T_w)D_h^{n-1}$ for T and $k_0 u_e^{n+1}/D_h^n q$ for $H2$ boundary conditions]
C	defined by equation (8)
C_p	heat capacity
D	defined by equation (8)
D_h	hydraulic diameter [$= 1.222\ R$]
E	defined by equation (8)
f	friction factor [$= (\tau_w/\frac{1}{2}\rho u_e^2)(1/4X)$]
f_{app}	apparent friction factor
$f(T)$	temperature dependence function of the consistency index defined by equation (2)
$F(\theta)$	dimensionless temperature dependence function of the consistency index defined by equations (11) and (12)
F	defined by equation (8)
g	gravity acceleration
G	defined by equation (8)
H	defined by equation (8)
K	thermal conductivity
k_0	consistency index at reference temperature
l	peripheral distance
L	dimensionless peripheral distance of the channel [$= l/D_h$]
n	power law index
Nu_m	mean Nusselt number $[(1/X)\int_0^x Nu_x\, dX]$
Nu_x	local Nusselt number $[(\partial\theta/\partial S)_w/\theta_{w,m} - \theta_{b,x}$ for $H2$ and $(\partial\theta/\partial S)_{w,m}/\theta_{b,x}$ for T boundary conditions]
p	pressure
P	dimensionless pressure $[(p-\rho gz)/\rho u_e^2]$
Δp	axial pressure drop [$= p_e - p$]
Pe	Peclet number [$= \rho C_p u_e D_h/K$]
Pr	Prandtl number $[= k_0 C_p (u_e/D_h)^{n-1}/K]$
q	heat flux
Q_x	dimensionless heat flux [$= q_x/q_w$]
r	radial coordinate
R	radius of the channel
R^*	dimensionless radial coordinate [$= r/D_h$]
Re	Reynolds number [$= \rho u_e^{2-n} D_h^n/k_0$]
S	dimensionless normal distance
T	temperature
u	axial velocity
U	dimensionless axial velocity [$= u/u_e$]
U_{max}	dimensionless maximum velocity
v	velocity in y direction
V	dimensionless velocity in y direction [$= v/u_e$]
w	velocity in z direction
W	dimensionless velocity in z direction [$= w/u_e$]
x	axial distance
X	dimensionless axial distance [$= x/D_h$]
x^+	dimensionless axial coordinate [$= x/D_h Re$]
x^*	dimensionless axial coordinate [$= x/D_h Pe$]
y	transverse distance
Y	dimensionless transverse distance [$= y/D_h$]
z	transverse coordinate
Z	dimensionless transverse distance [$= z/D_h$].

Greek symbols

α	circumferential angle from the bottom plate and from the origin of the channel
Δ	rate of deformation tensor in Cartesian coordinates
θ	dimensionless temperature [$= (T - T_w)/(T_e - T_w)$ for T and $= (T - T_e)/(qD_h/K)$ for $H2$ boundary conditions]
$\theta_{b,x}$	dimensionless bulk temperature evaluated at x axial position
Π	defined by equation (8)
ρ	density
τ	shear stress tensor
τ_w	wall shear stress
φ	apex angle.

Subscripts

b	evaluated at bulk condition
e	evaluated at inlet condition
fd	fully developed condition
$H2, x$	evaluated at local x position for $H2$ boundary condition
m	mean value
T, x	evaluated at local x position for T boundary condition
x	evaluated at local x position
w	evaluated at wall condition.

non-Newtonian fluids in a circular duct with the twisted tape inserted with the T boundary condition.

Lawal and Mujumdar [19] and Etemad *et al.* [20, 21] showed that assumption of constant viscosity exhibits substantial deviation from variable viscosity results. Also the effect of viscous dissipation can be very significant (depending on the Brinkman number). Generally the entrance region is also very important and a major fraction of pressure drop and total heat transfer occur in this region of channels. In spite of the importance of non-Newtonian fluids in industrial applications, there does not appear to be a simultaneously developing fluid flow and heat transfer solution for non-Newtonian fluids flowing through semi-circular ducts.

This numerical study is concerned with the simultaneous development of flow and heat transfer for power law fluids. It covers the effects of power law indices, variable viscosity, viscous dissipation and Prandtl number for two different boundary conditions (T and $H2$).

Problem statement

The problem to be considered is depicted schematically in Fig. 1. The origin of the coordinate system is fixed at the middle of the bottom plate of the semi-circular duct. The symmetry of the cross section permits the restriction of the solution to only half the channel.

Two types of thermal boundary conditions (T and $H2$) were examined. All fluid properties are held constant except viscosity. The Ostwald-de waele power law is used to model shear stress in the following form:

$$\tau = k_0 f(T)|\Delta : \Delta|^{n-1/2}\Delta \tag{1}$$

where k_0 is the consistency index at reference temperature (T_0) while $f(T)$ specifies the temperature dependence of the consistency index as follows:

$$f(T) = e^{B'(T-T_0)}. \tag{2}$$

The dimensionless governing equations in Cartesian coordinates can be written as:

continuity

$$\frac{\partial U}{\partial X} + \frac{\partial V}{\partial Y} + \frac{\partial W}{\partial Z} = 0 \tag{3}$$

x-momentum

$$U\frac{\partial U}{\partial X} + V\frac{\partial U}{\partial Y} + W\frac{\partial U}{\partial Z} = -\frac{\partial P}{\partial X} + \frac{1}{Re}\left(\frac{\partial C}{\partial X} + \frac{\partial D}{\partial Y} + \frac{\partial E}{\partial Z}\right) \tag{4}$$

y-momentum

$$U\frac{\partial V}{\partial X} + V\frac{\partial V}{\partial Y} + W\frac{\partial V}{\partial Z} = -\frac{\partial P}{\partial Y} + \frac{1}{Re}\left(\frac{\partial F}{\partial Y} + \frac{\partial D}{\partial X} + \frac{\partial G}{\partial Z}\right) \tag{5}$$

z-momentum

$$U\frac{\partial W}{\partial X} + V\frac{\partial W}{\partial Y} + W\frac{\partial W}{\partial Z} = -\frac{\partial P}{\partial Z} + \frac{1}{Re}\left(\frac{\partial H}{\partial Z} + \frac{\partial G}{\partial Y} + \frac{\partial E}{\partial X}\right) \tag{6}$$

energy

$$U\frac{\partial \theta}{\partial X} + V\frac{\partial \theta}{\partial Y} + W\frac{\partial \theta}{\partial Z} = \frac{1}{Pe}\left(\frac{\partial^2\theta}{\partial X^2} + \frac{\partial^2\theta}{\partial Y^2} + \frac{\partial^2\theta}{\partial Z^2}\right) + \frac{Br}{Pe}\left[C\frac{\partial U}{\partial X} + F\frac{\partial V}{\partial Y} + H\frac{\partial W}{\partial Z} + D\left(\frac{\partial U}{\partial Y} + \frac{\partial V}{\partial X}\right) + E\left(\frac{\partial U}{\partial Z} + \frac{\partial W}{\partial X}\right) + G\left(\frac{\partial V}{\partial Z} + \frac{\partial W}{\partial Y}\right)\right] \tag{7}$$

where

$$\frac{\Pi}{2} = \left\{2\left[\left(\frac{\partial U}{\partial X}\right)^2 + \left(\frac{\partial V}{\partial Y}\right)^2 + \left(\frac{\partial W}{\partial Z}\right)^2\right] + \left(\frac{\partial U}{\partial Y} + \frac{\partial V}{\partial X}\right)^2 + \left(\frac{\partial W}{\partial Y} + \frac{\partial V}{\partial Z}\right)^2 + \left(\frac{\partial U}{\partial Z} + \frac{\partial W}{\partial X}\right)^2\right\}$$

$$C = 2\left(\frac{\Pi}{2}\right)^{(n-1)/2}\frac{\partial U}{\partial X}F(\theta)$$

$$D = \left(\frac{\Pi}{2}\right)^{(n-1)/2}\left(\frac{\partial U}{\partial Y} + \frac{\partial V}{\partial X}\right)F(\theta)$$

$$E = \left(\frac{\Pi}{2}\right)^{(n-1)/2}\left(\frac{\partial U}{\partial Z} + \frac{\partial W}{\partial X}\right)F(\theta)$$

$$F = 2\left(\frac{\Pi}{2}\right)^{(n-1)/2}\frac{\partial V}{\partial Y}F(\theta)$$

$$G = \left(\frac{\Pi}{2}\right)^{(n-1)/2}\left(\frac{\partial V}{\partial Z} + \frac{\partial W}{\partial Y}\right)F(\theta)$$

$$H = 2\left(\frac{\Pi}{2}\right)^{(n-1)/2}\frac{\partial W}{\partial Z}F(\theta). \tag{8}$$

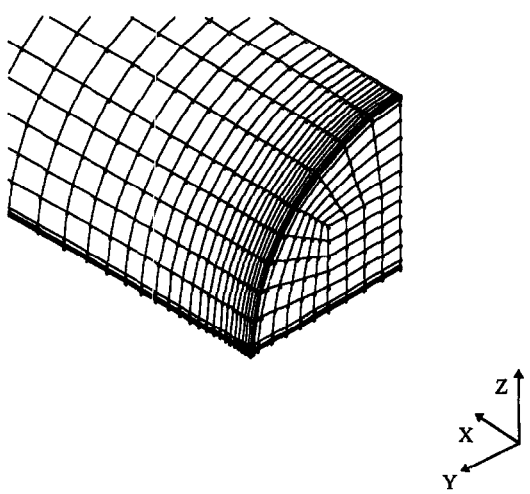

Fig. 1. Channel geometry and grid points.

The dimensionless parameters are defined as follows:

$$U=\frac{u}{u_e} \quad V=\frac{v}{u_e} \quad W=\frac{w}{u_e}$$

$$X=\frac{x}{D_h} \quad Y=\frac{y}{D_h} \quad Z=\frac{z}{D_h}$$

$$P=\frac{p-\rho gz}{\rho u_e^2} \quad Re=\frac{\rho u_e^{2-n} D_h^n}{k_0} \text{ and } Pr=\frac{k_0 C_p \left(\frac{u_e}{D_h}\right)^{n-1}}{K} \tag{9}$$

$$x^*=\frac{X}{Re\,Pr}=\frac{x^+}{Pr}. \tag{10}$$

Dimensionless variables for different boundary conditions are defined as follows:

for the constant wall temperature (T)

$$\theta=\frac{T-T_w}{T_e-T_w} \quad Br=\frac{k_0 u_e^{n+1}}{D_h^{n-1}(T_e-T_w)K}$$

$$F(\theta)=e^{B'\theta(T_e-T_w)}=e^{B\theta} \text{ and } Nu_x=\frac{\left(\frac{\partial\theta}{\partial S}\right)_{w,m}}{\theta_{b,x}} \tag{11}$$

for constant wall heat flux (both axially and peripherally) ($H2$)

$$\theta=\frac{T-T_e}{\frac{qD_h}{K}} \quad Br=\frac{k_0 u_e^{n+1}\left(\frac{1}{D_h}\right)^n}{q}$$

$$F(\theta)=e^{B'\theta q(D_h/K)}=e^{B\theta} \text{ and } Nu_x=\frac{\left(\frac{\partial\theta}{\partial S}\right)_{w,m}}{\theta_{w,m}-\theta_{b,x}} \tag{12}$$

where the peripheral mean wall temperature $\theta_{w,m}$ at an arbitrary cross section is defined as

$$\theta_{w,m}=\frac{1}{p'}\int_T \theta_w \,dL \tag{13}$$

and

$$\theta_{b,x}=\frac{\int \theta U\,dA}{\int U\,dA}. \tag{14}$$

The heat flux is nondimensionalized in terms of heat flux on one wall ($Q_x=q_x/q_w$).

The hydrodynamic entrance length is defined here as the length of the duct which is required to achieve maximum velocity within 99% of the corresponding fully developed value. The Fanning friction factor, f, is defined as the ratio of the local wall shear stress to the fluid kinetic energy per unit volume. For a fully developed flow

$$f=\frac{\tau_w}{\frac{1}{2}\rho u_e^2}=\frac{\Delta p}{\frac{1}{2}\rho u_e^2}\frac{1}{4X}. \tag{15}$$

In the entrance region f is often called the apparent friction factor, f_{app}, and is based on the total pressure drop over the axial length from $X=0$ to $X=X$.

The mean Nusselt number over length X measured from the inlet is given by

$$Nu_m=\frac{1}{X}\int_0^X Nu_x\,dX. \tag{16}$$

The fluid enters the duct with uniform velocity and temperature profiles. Thus:

$$X=0\begin{cases} U=1 \quad V=0 \quad W=0 \\ \theta=1 \quad \text{for } T \text{ boundary condition} \\ \theta=0 \quad \text{for } H2 \text{ boundary condition.} \end{cases} \tag{17}$$

The no slip condition is applied at the channel walls. The dimensionless temperature at the walls for the T boundary condition is zero and for $H2$ boundary condition the dimensionless heat flux at both walls is unity. The velocity gradient across the symmetry plane is zero except for the y direction, for which the velocity at the symmetry plane is zero. Also the temperature gradient at the symmetry plane is zero. A fully developed condition could be prescribed at the outlet boundary due to the long length of the plates (120 times the hydraulic diameter) and also the high Peclet number (500–5000) and relatively high Reynolds number values (500).

Equations (3)–(7), which are an elliptic system of partial differential equations with associated boundary conditions, were solved using FIDAP (a fluid dynamic and heat transfer analysis package, based on Galerkin finite element method). The Galerkin finite element method is well documented in the literature e.g. Zienkiewicz [22], Pittman [23] and Engleman [24].

RESULTS AND DISCUSSION

The flow domain was discretized and the governing equations were converted into algebraic equations using $61\times13\times17$ grids of eight-node quadratic bricks. The number of meshes was based on the requirement of mesh independence of the solution. Penalty approach was chosen for the pressure with the penalty parameter set at 10^{-9} to satisfy continuity without solving an additional partial differential equation. Due to the higher velocity and temperature gradients in the entrance region and in the vicinity of the walls, finer mesh distributions were used in these regions. The solution of the set of algebraic equations available from the discretization of governing equations is the most time consuming stage of the solution, so the solution algorithm is very important. Due to

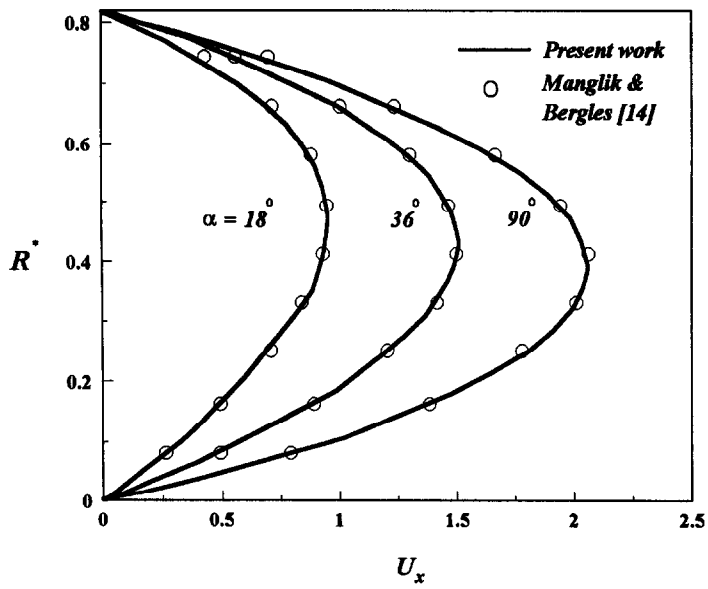

Fig. 2. Comparison of the fully developed velocity profile at different circumferential locations.

the high radius of convergence of the fixed iteration method and also the high rate of convergence for quasi-Newton–Raphson, the combination strategy used to solve the algebraic equations starts with the fixed iteration method with a high relaxation factor and then switches to the quasi-Newton–Raphson approach with a smaller relaxation factor. The combination strategy results in a significant saving in computational time. The Petrov–Galerkin formulation (streamline upwinding) was used to improve numerical instability. The convergence criterion was set at 10^{-4} relative difference between successive solution vectors and also the relative residual.

The numerical procedure was tested by comparing predictions with available analytical and numerical solutions. Figure 2 shows the excellent agreement between the fully developed axial velocity profile at different circumferential locations obtained from the present investigation and the results of Manglik and Bergles [14].

The fully developed friction factor from Hu [5], Lei and Trupp [8], Ben-Ali *et al.* [12] and that obtained in the present work are compared in Table 1. Also this table shows the comparison of the fully developed maximum axial velocity with the analytical solution of Lei and Trupp [8]. The present computation results agree well with other available data.

The present results for Nusselt numbers of Newtonian fully developed flow and heat transfer are tabulated in Table 2. From this table values of the Nusselt numbers are seen to be very close to those numerically obtained by Ben-Ali *et al.* [12], Trupp and Lau [11], and analytically by Hu [5] and, Trupp and Lei [10].

(a) *Effect of power law index*

The dimensionless center plane axial velocity profiles at different axial locations, maximum axial velocity and apparent friction factor are presented in Fig. 3(a)–(d) for different values of n, while the data for apparent and also fully developed friction factors are tabulated at Table 3. Also velocity vectors for cross-stream flow for different power law indices are presented in Fig. 4. Close to the walls, the velocity and velocity gradient of the pseudoplastic fluid is higher than that of a dilatant fluid at the same Reynolds

Table 1. Comparison of the $f \cdot \mathrm{Re}$ and $U_{\max}$ for semi-circular duct at fully developed condition

	$(f \cdot Re)_{\mathrm{f.d.}}$	$U_{\max}$
Hu [5]	15.767	2.0613
Lei and Trupp [8]	15.767	—
Ben-Ali *et al.* [12]	15.790	—
Present work	15.860	2.0584

Table 2. Comparison of the Nusselt numbers (T and $H2$ boundary condition) for semi-circular duct at fully developed condition

	Nu_T	Nu_{H2}
Hu [5]	—	2.923
Trupp and Lau [11]	3.316	—
Trupp and Lei [10]	—	2.920
Ben-Ali *et al.* [12]	3.316	2.930
Present work	3.318	2.920

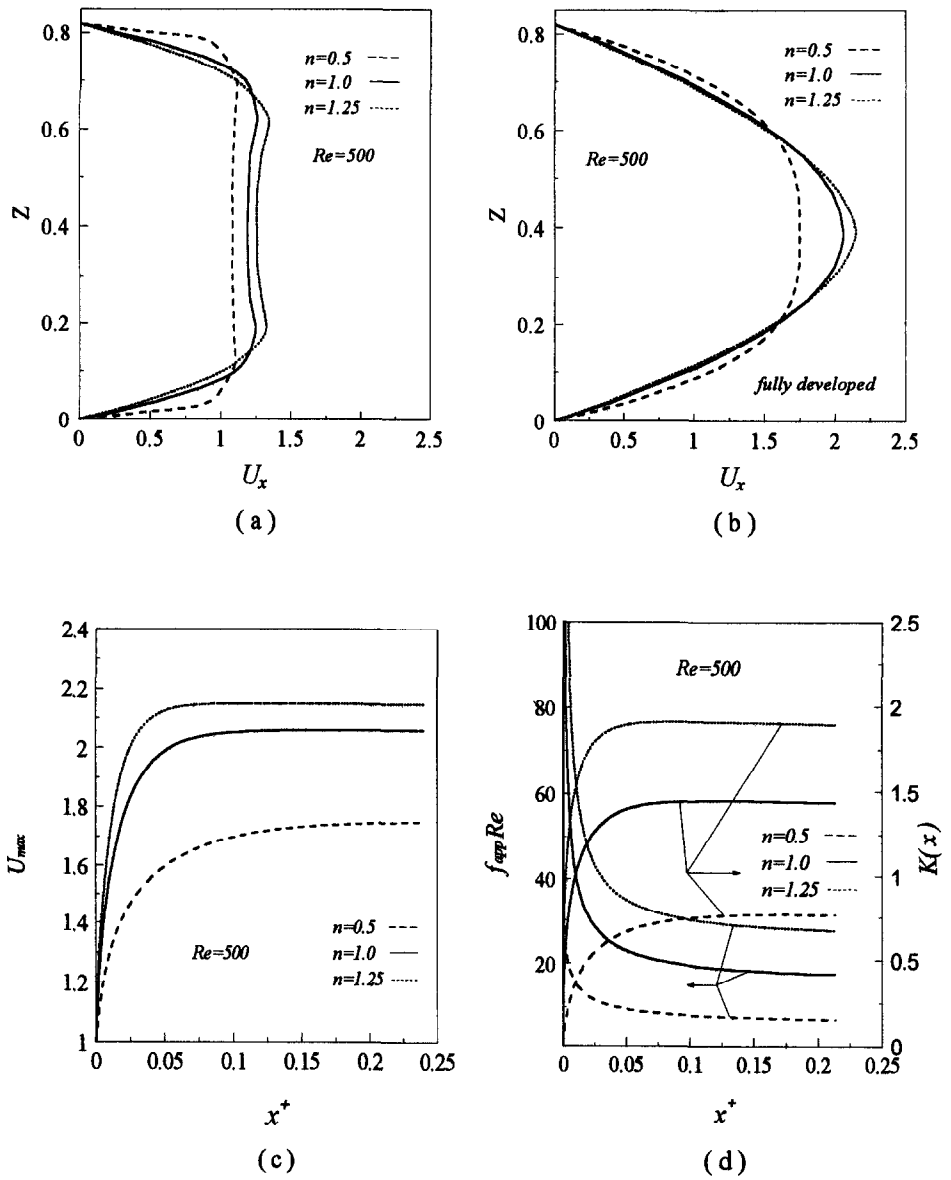

Fig. 3. The effect of power law index on dimensionless center-plane axial velocity profile, maximum velocity and friction factor.

Table 3. $f_{app} \cdot Re$ at different axial locations for different power law indices, different temperature–viscosity constants, and also various boundary conditions

			$f_{app} \cdot Re$				
x^+	$n = 0.5$	$n = 1.0$	$n = 1.25$	$n = 0.5$ $B = 0.5$ *T B.C.*	$n = 0.5$ $B = 1.5$ *T B.C.*	$n = 0.5$ $B = -0.5$ *H2 B.C.*	$n = 0.5$ $B = -1.5$ *H2 B.C.*
0.002	24.860	86.872	147.089	26.172	30.833	24.706	24.402
0.0229	11.992	29.526	44.734	12.902	15.836	11.761	11.320
0.1056	7.998	19.349	29.889	8.914	11.426	7.665	7.068
$(f \cdot Re)_{f.d.}$	6.223	15.860	25.365	—	—	—	—

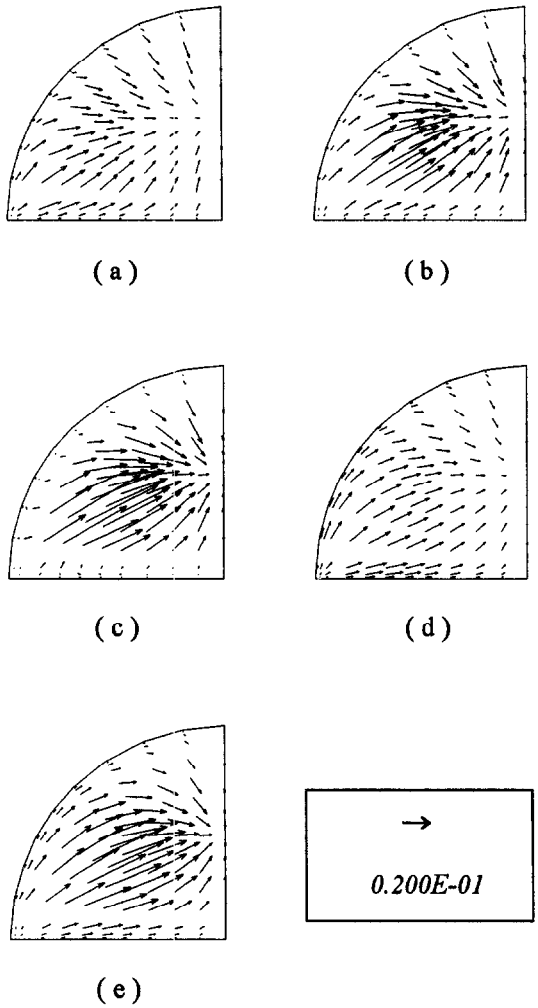

Fig. 4. Secondary flow vectors for different power law indices and different temperature–viscosity coefficients at $x^+ = 0.002$ for $Re = 500$ and $Pr = 10$. (a) $n = 0.5$; (b) $n = 1.0$; (c) $n = 1.25$; (d) $n = 0.5$ and $B = 1.5$ (T B.C.); (e) $n = 1.0$ and $B = 1.5$ (T B.C.).

number (Fig. 3). The reason is the lower apparent viscosity for a pseudoplastic fluid than that for a shear-thickening fluid (for the same value of shear rate and consistency index). Requirement of mass conservation forces the fluids to correspondingly slow down in the core of the duct. Further downstream, due to the propagation of the viscous effect to the center plane of the channel, the influence of the power law index diminishes. As seen from Fig. 3(c), the maximum velocity for different power law indices increases with increase of axial distance which shows flow development. Also the maximum velocity decreases with decreasing the power law index.

From Fig. 4, the secondary flow close to the walls is very weak for all fluids. Also for the fluids with smaller power law index, the secondary flows far from the walls are relatively weak which is due to the flatter axial velocity profile for these fluids within the core.

The maximum velocity does not occur at the centeroid and the location is the same as documented by Lei and Trupp [8] ($Z = 0.39297$).

Results (Table 3) indicate the important role of entrance region on the apparent friction factor. For example at $x^+ = 0.002$, $f \cdot Re$ is 300, 448 and 480% higher than its fully developed value for $n = 0.5$, 1.0 and 1.25, respectively. This is due to the higher velocity gradient near the wall in the entrance region, which results in a higher pressure drop. The reason for the larger difference for higher n is related to the higher apparent viscosity for these power law fluids. The higher velocity gradient close to the wall in the developing region causes more heat transfer in this section of the channel. For example for $n = 0.5$ at $x^* = 0.0002$, the Nusselt number shows 675 and 1044% enhancement related to the fully developed values for T and $H2$ boundary conditions, respectively. These emphasize the importance of simultaneously developing flow and heat transfer.

Figure 5(a)–(b) presents the dimensionless circumferential wall temperature profile for $H2$ and the dimensionless circumferential heat flux for T boundary condition and for different power law indices.

For $H2$ boundary condition close to the corners, due to the heating effect from two walls and also the small velocity in this region, the fluid temperature is higher than that close to the middle of the walls (Fig. 5b). Thus the maximum wall temperature occurs at the corners and the minimum temperature in the middle of the bottom plate. Also, because of the constant heat flux around the periphery and the higher wall temperature at the corners, the peripheral average wall temperature increases, which causes a reduction of Nu_{H2} relative to its counterpart in geometries without sharp corners (parallel plates and circular duct). For the $H2$ boundary condition, the heat flux is the same for different power law indices, therefore difference in velocity profiles for different ns cannot affect the fluid temperature. Due to the higher velocity gradient (Fig. 3) for lower power law index, the circumferential wall temperature (Fig. 5(b)) increases with n, which shows higher heat transfer for lower n values. Far from the inlet the velocity gradient close to the wall decreases, resulting in higher circumferential wall temperature, and therefore heat transfer diminishes with axial distance.

For the T boundary condition, due to the higher fluid temperature close to the corners (lower dimensionless temperature), the heat flux close to the corners is smaller (Fig. 5(a)). So the minimum heat flux occurs at the corners and the maximum wall heat flux in the middle of the bottom plate. Lower heat flux from corners causes a lower Nusselt number relative to ducts without sharp corners. The higher velocity gradient and also higher secondary flow close to the walls for lower n results in higher heat flux for pseudoplastic fluids (Fig. 5(a)).

Generally for T boundary condition the temperature of the fluid close to the walls approaches the

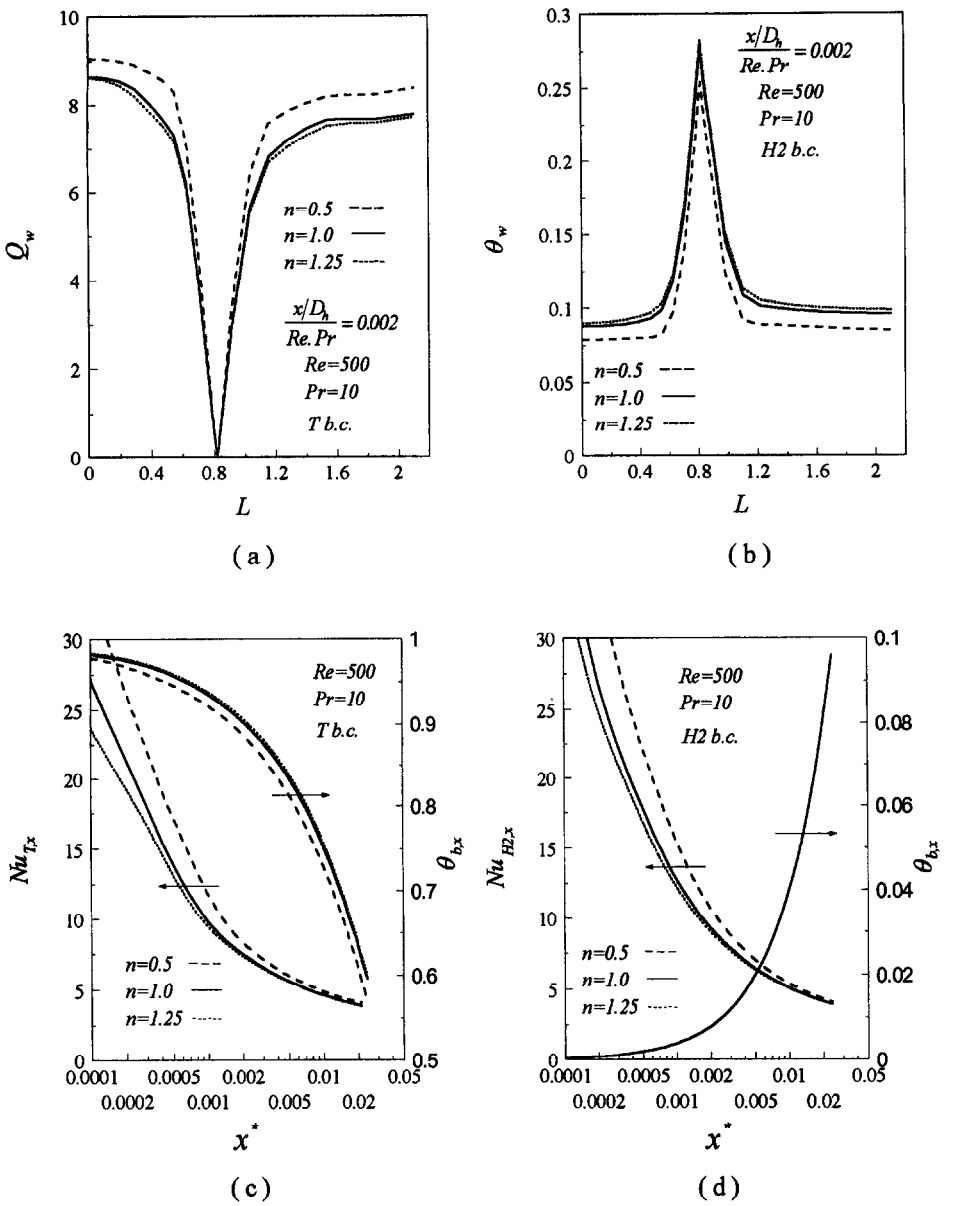

Fig. 5. The effect of power law index on heat transfer characteristics. (a) dimensionless circumferential wall heat flux for T boundary condition. (b) dimensionless circumferential wall temperature for $H2$ boundary condition. (c) Nusselt number and dimensionless bulk temperature for T boundary condition. (d) Nusselt number and dimensionless bulk temperature for $H2$ boundary condition.

wall temperature, so the temperature gradient of the fluid at the wall is smaller for the T boundary condition than that for the constant heat flux boundary condition; this results in a lower Nusselt number for the former. This difference in Nusselt numbers for a duct with sharp corner is smaller and sometimes (depending on the geometry) the Nusselt number for $H2$ is less than that for T boundary conditions.

The peripherally averaged local and also fully developed Nusselt numbers for different power law indices and for various boundary conditions are presented in Fig. 5(c)–(d) and Tables 4 and 5. The steeper velocity gradient and higher secondary flows in the wall region for lower n values (Figs. 3 and 4) cause enhancement of the Nusselt number but this magnitude of the enhancement decreases further downstream. For example at $x^* = 0.0002$ the Nusselt number for $n = 0.5$ is 22.7 and 28.6% higher than that for Newtonian fluids for T and $H2$ boundary conditions, respectively. These values decrease to 4.9 and 4.0% at fully developed condition.

(b) *Effect of variable apparent viscosity*

The apparent viscosity of most liquids decreases with increase in temperature. Thus for the case of heating the temperature–viscosity coefficient (B) is

Table 4. Nusselt numbers at different axial locations for different power law indices, different temperature–viscosity constants and various Brinkman numbers for T boundary condition

				$Nu_{T,x}$				
x^*	$n = 0.5$ $Pr = 10$	$n = 1.0$ $Pr = 10$	$n = 1.25$ $Pr = 10$	$n = 0.5$ $B = 0.5$	$n = 0.5$ $B = 1.5$	$n = 0.5$ $Br = -0.5$	$n = 0.5$ $Br = -2.0$	$n = 0.5$ $Pr = 1.0$
0.00020	26.952	21.957	19.533	28.309	31.756	25.964	21.032	38.486
0.00229	7.872	7.172	7.039	8.445	9.902	6.797	3.443	10.610
0.01056	4.805	4.567	4.535	5.135	5.695	3.358	−1.901	5.481
$(Nu_T)_{f.d.}$	3.480	3.318	3.265	—	—	—	—	3.480

Table 5. Nusselt numbers at different axial locations for different power law indices, different temperature–viscosity constants and various Brinkman numbers for $H2$ boundary condition

				$Nu_{H2,x}$				
x^*	$n = 0.5$ $Pr = 10$	$n = 1.0$ $Pr = 10$	$n = 1.25$ $Pr = 10$	$n = 0.5$ $B = -0.5$	$n = 0.5$ $B = -1.5$	$n = 0.5$ $Br = 0.5$	$n = 0.5$ $Br = 2.0$	$n = 0.5$ $Pr = 1.0$
0.00020	34.739	27.022	24.947	34.840	35.062	12.590	4.313	47.895
0.00229	10.014	8.793	8.535	10.169	10.463	5.171	2.115	14.814
0.01056	5.269	4.989	4.957	5.419	5.706	2.93537	1.259	6.846
$(Nu_{H2})_{f.d.}$	3.038	2.920	2.880	—	—	—	—	3.038

positive for T and negative for $H2$ boundary conditions.

The effect of variable viscosity on the dimensionless center plane axial velocity profile as well as dimensionless maximum velocity and apparent friction factor can be found from Fig. 6(a)–(d). The effect of variable viscosity on secondary flows for T boundary condition can be found from Fig. 4.

In the heating case for both T and $H2$ boundary conditions, due to the high temperature in the wall region, the apparent viscosity of the fluid in this region decreases, which causes higher velocity and also higher velocity gradient near the wall and hence lower maximum velocities (Fig. 6). This leads to enhanced heat transfer. Also the higher secondary flow close to the walls is the result of temperature dependent viscosity (for T boundary condition).

Figure 7(a)–(d) and Tables 4 and 5 present the effect of temperature dependent viscosity on Nusselt number for different boundary conditions.

The effect of variable viscosity is not the same for different boundary conditions. For T boundary conditions $(T_w - T_{b,x})$ is very large at the entrance, which introduces a large effect of variable viscosity in this region. Further downstream this difference decreases gradually thus retarding the effect of variable viscosity. At $x^* = 0.0002$ for $n = 0.5$ considering variable viscosity ($B = 1.5$), shows a 17.8% increase in Nusselt number, while it decreases to 18.5% at $x^* = 0.01056$. This enhancement illustrates the importance of variable viscosity effects for this boundary condition.

The effect of temperature-dependent apparent viscosity on heat transfer is not as noticeable for the constant heat flux boundary conditions as it is for the constant wall temperature situations. For $H2$ boundary conditions, $(T_{w,m} - T_{b,x})$ is small in the entrance region and increases gradually in the axial direction. Therefore the effect of variable viscosity on velocity profile is small in the entrance region but increases further downstream. Far from the inlet, increase of velocity close to the walls causes a decrease in the maximum velocity (Fig. 6b). The enhancement of heat transfer is very small in the entrance region relative to that for T type boundary conditions. For example Nusselt number for $n = 0.5$ increases by 0.9 and 8.3% for $B = -1.5$ ($H2$ boundary condition), but by 17.8 and 18.5% for $B = 1.5$ (T boundary condition) at $x^* = 0.0002$ and $x^* = 0.01056$, respectively. As shown in Fig. 7 and Tables 4 and 5, the Nusselt number increases as B increases for T boundary conditions, but decreases as B decreases for $H2$ boundary conditions.

Table 3 shows the effect of variable viscosity on the apparent friction factor for different boundary conditions. In the case of the T boundary condition the reference temperature for viscosity is the temperature at the walls. When the variable viscosity (heating case) is considered, the average viscosity in the momentum boundary layer is higher than that for the case of constant viscosity, which causes a higher pressure drop and consequently higher friction factor. For $H2$ boundary condition the inlet temperature is chosen as a reference temperature, therefore considering variable viscosity results in lower pressure drop. For example, at $x^+ = 0.1056$, the friction factor for $n = 0.5$ and T boundary condition is increased by 42.9% for $B = 1.5$ but for $H2$ boundary condition it decreases by 4.2% for $B = -1.5$.

(c) *Effect of viscous dissipation*

The Brinkman number is chosen as a criterion which shows the relative importance of viscous dissipation.

The effect of viscous dissipation on the dimen-

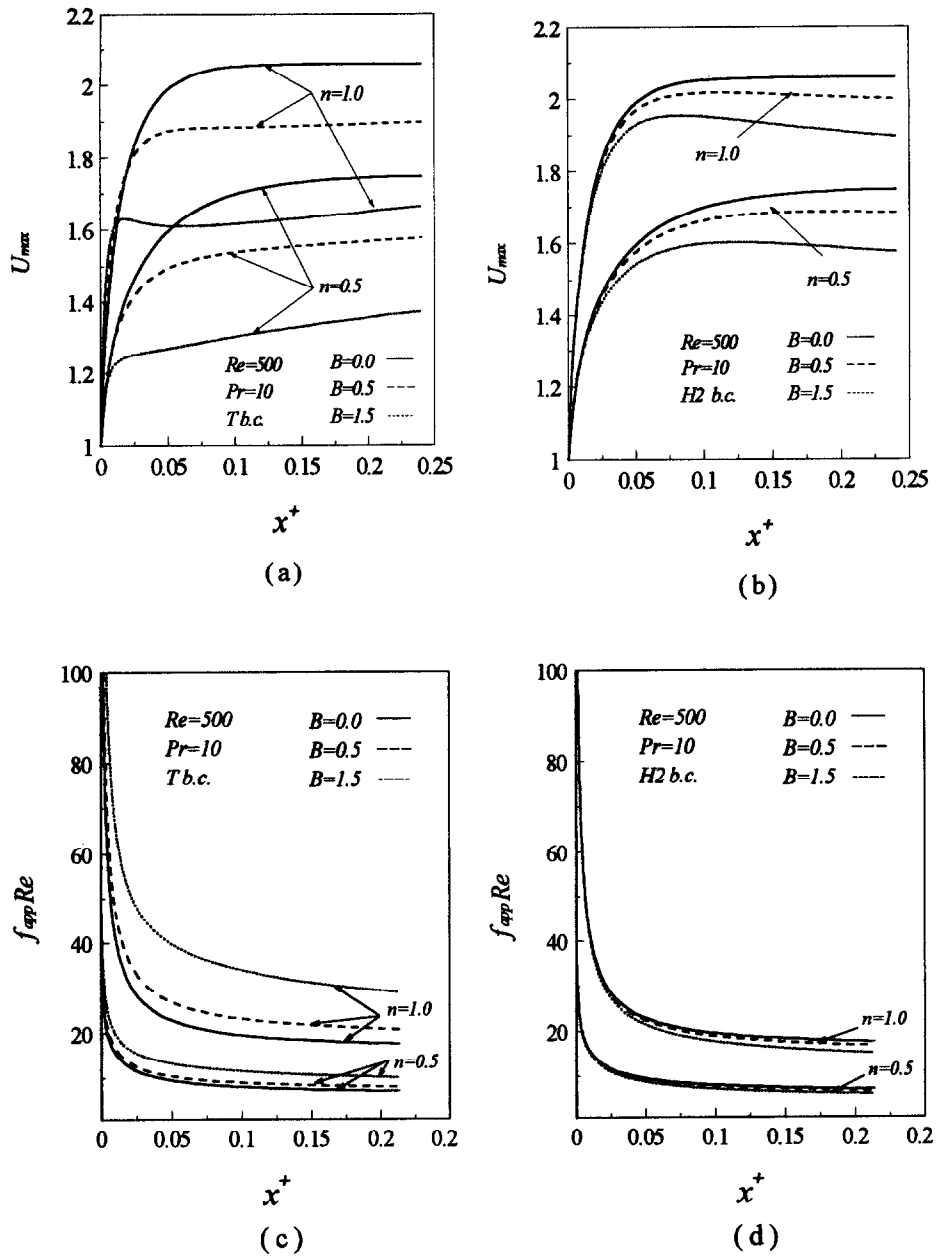

Fig. 6. The effect of variable viscosity on the dimensionless maximum velocity and apparent friction factor for different boundary conditions.

sionless temperature profile is displayed in Fig. 8(a)–(b), while the bulk temperature and Nusselt number variations for different boundary conditions and for different Brinkman numbers are presented in Fig. 8(c)–(d) and Tables 4 and 5.

In the case of T boundary condition the Brinkman number is negative for heating and positive for cooling. Since the highest shear rate occurs near the wall, the effect of viscous dissipation is most significant in this region. For T boundary condition viscous heating increases the bulk temperature (decreases dimensionless bulk temperature), which results in a decrease of the local Nusselt number. Due to the high temperature difference between wall and fluid in the entrance region, viscous heating has only a slight effect on the Nusselt number. Further downstream, for low Brinkman numbers, due to the combined effects of viscous dissipation and wall heating, the temperature of the fluid close to the wall approximates the wall temperature, so the temperature gradient at the wall is nearly zero; the local Nusselt number therefore approaches zero. At a location farther downstream, the temperature gradient at the wall becomes negative while the wall temperature is greater than the bulk temperature; this leads to negative values for the local Nusselt number. This indicates a reversal in the direc-

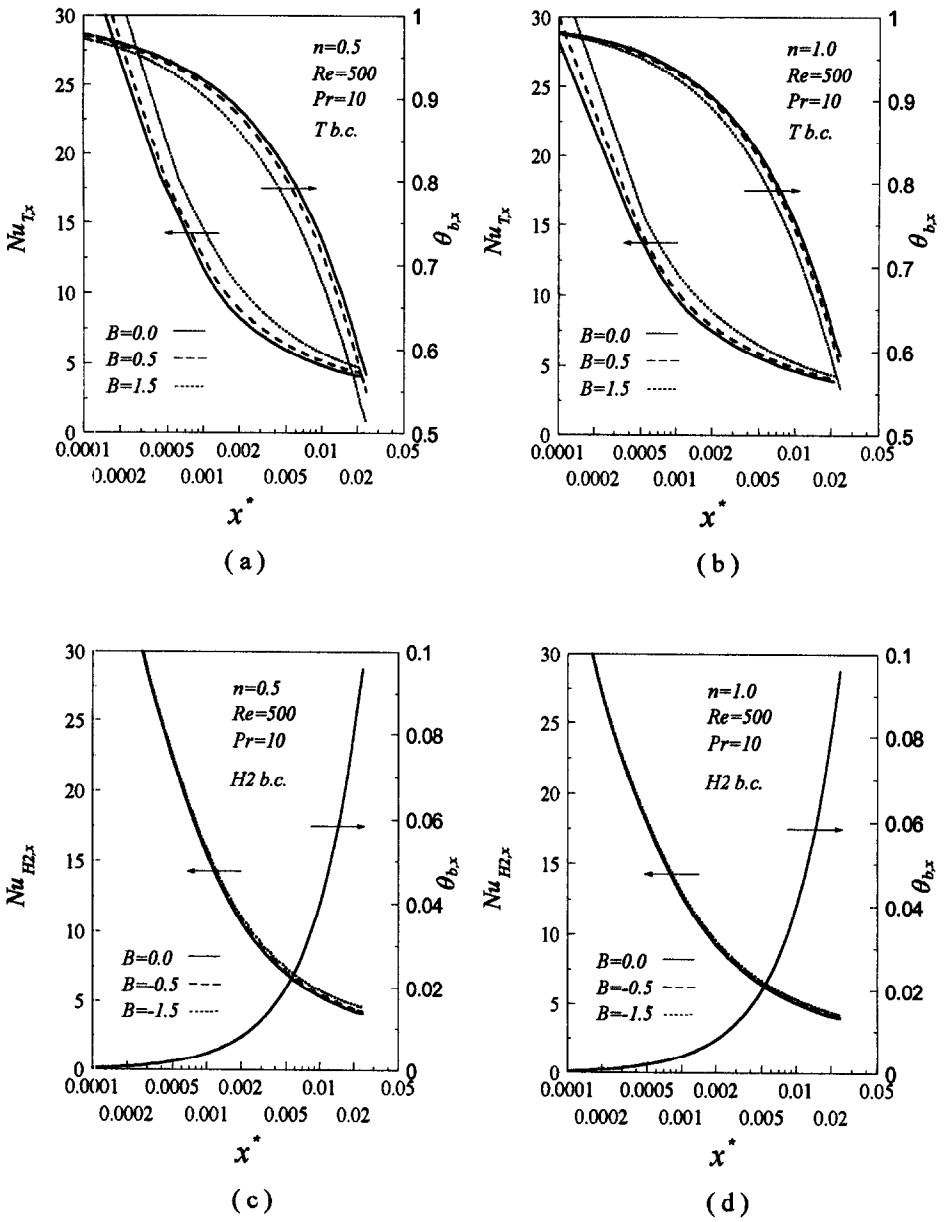

Fig. 7. The effect of variable viscosity on local Nusselt number for different boundary conditions.

tion of the heat flux. As the fluid proceeds downstream the fluid bulk temperature increases continuously and finally becomes the same as the wall temperature. Consequently, the Nusselt number becomes infinite. Figure 9(a)–(b) shows the local Nusselt number, dimensionless bulk temperature and the dimensionless heat flux through the wall for a very long duct (800 times the hydraulic diameter for T boundary condition and $Br = -2$). As shown in this figure far from $X = 0$, $T_{b,x} > T_w$, so the dimensionless bulk temperature is negative. Also, due to the negative heat flux in this region the Nusselt number becomes positive again and decreases with increasing axial distance. At locations very far from the inlet, increases in the dimensionless bulk temperature as well as dimensionless heat flux become very small and Nusselt number approaches to an asymptotic value. Figure 8(c) indicates that for a specific Brinkman number the attainment of the asymptotic Nusselt number requires infinitely long duct length.

For the constant heat flux boundary condition, the Brinkman number is positive for heating. Since the temperature difference between the wall and the fluid is very small in the entrance region, and viscous heating is greater in the inlet region, the largest effect of the viscous dissipation is felt in this region, which results in lowering of the Nusselt number. This effect decreases with downstream distance.

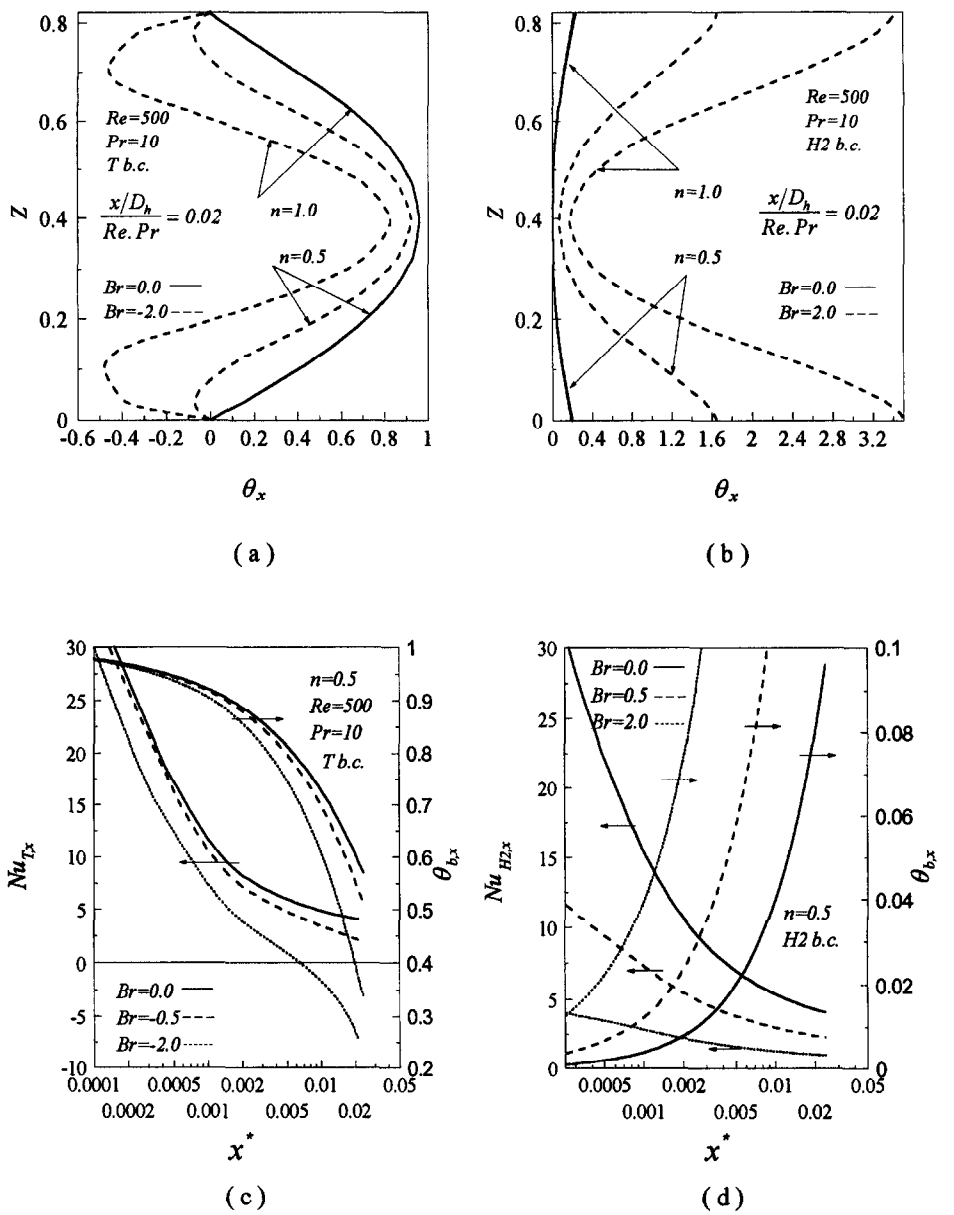

Fig. 8. The effect of viscous dissipation on heat transfer characteristics. (a) dimensionless center-plane temperature profiles for T boundary condition. (b) dimensionless center-plane temperature profiles for $H2$ boundary condition. (c) Nusselt number for T boundary condition. (d) Nusselt number for $H2$ boundary condition.

(d) *Effect of Prandtl number*

Figure 10(a)–(b) demonstrates the effect of Prandtl number on Nusselt number for different boundary conditions. Lower Prandtl number results in lower Nu_x in the entrance region. However Nu_x asymptotically approaches a fixed value far downstream, which is independent of Pr. It can be seen that the lower Prandtl number causes faster thermal development, which results in a higher fluid bulk temperature (lower dimensionless bulk temperature for the T type boundary conditions) and also lower dimensionless wall heat flux for type T boundary conditions. The competition between these two effects causes a lower heat transfer rate. As the fluid proceeds downstream this effect diminishes due to thermal development. For type $H2$ boundary conditions, lower Pr causes an increase in $(T_{w,m} - T_{b,x})$ which, in turn, results in a lower local Nusselt number. According to the definition of x^*, the lower Prandtl number case results in a higher Nusselt number over the entire length.

CONCLUSIONS

A numerical study based on the Galerkin finite element method was carried out on the steady laminar

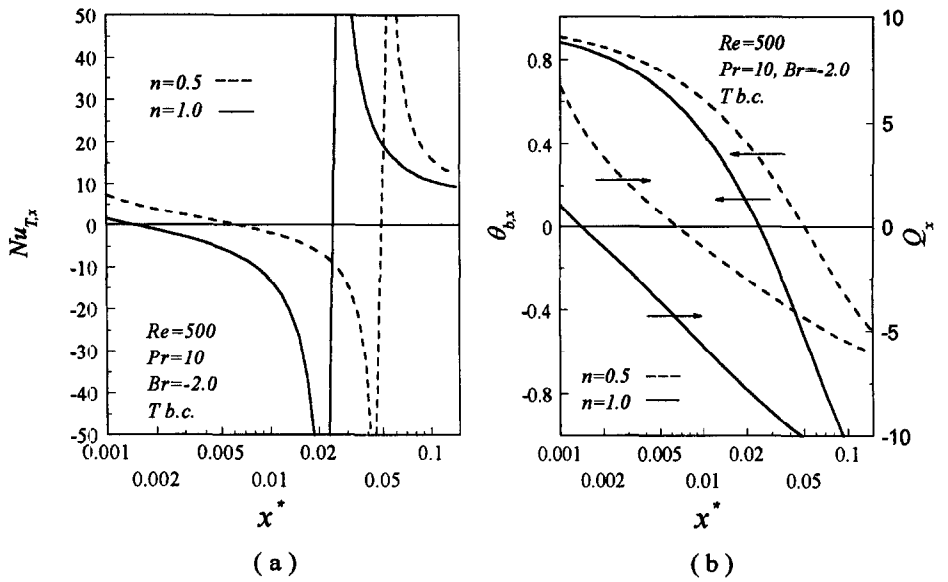

Fig. 9. Local Nusselt number, dimensionless bulk temperature and dimensionless heat flux for T boundary condition and $Br = -2.0$.

heat transfer in simultaneously developing flow of power law fluids through a semi-circular cross section duct. The comparison of the present results with available data for a Newtonian fluid in the fully developed case was excellent.

The effects of the power law index, temperature-dependent viscosity, viscous dissipation, and Prandtl number for both T and $H2$ boundary conditions were considered. The results show the importance of the non Newtonian behavior on the heat transfer and fluid flow characteristics. Temperature dependent viscosity is shown to have a significant effect on the local Nusselt number and also the pressure drop. For heating, the increase in the local Nusselt number for constant temperature boundary conditions is noticeably higher than that for the constant heat flux boundary conditions when the temperature dependence of fluid viscosity is included in the model.

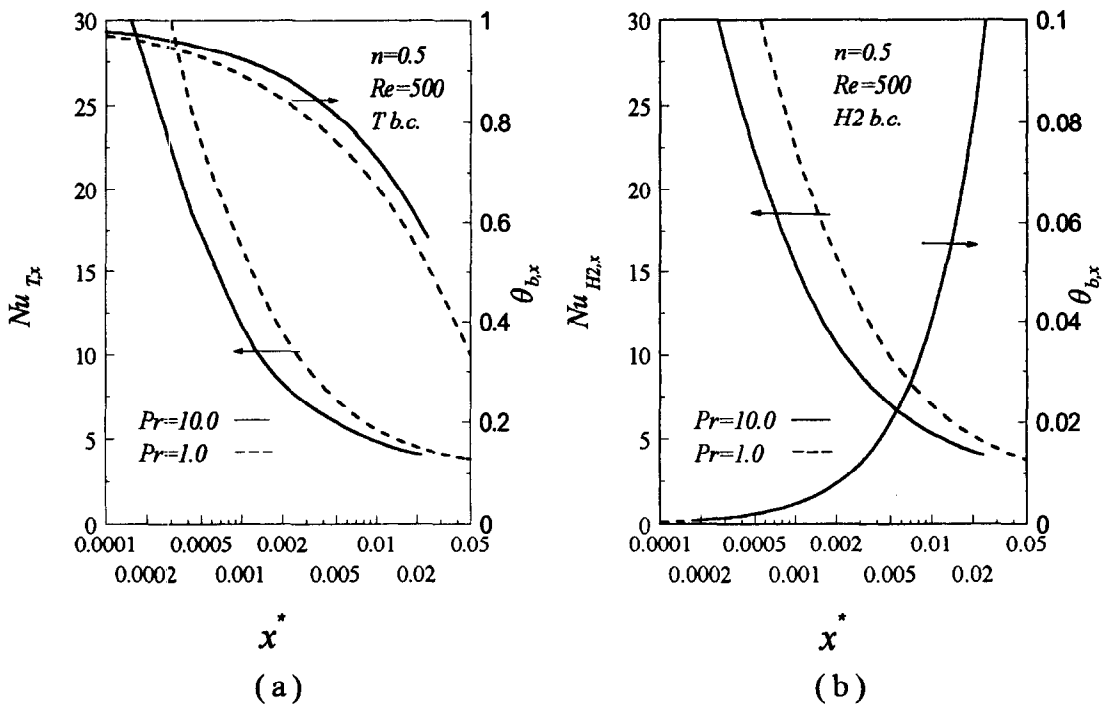

Fig. 10. The effect of Prandtl number on local Nusselt number for different boundary conditions.

As shown in previous studies with parallel plates and rectangular ducts [20,21], viscous heating has a very pronounced effect on heat transfer which can even change the direction of heat flux for the case of uniform temperature boundary conditions.

The results indicate that the lower the Prandtl number the lower the heat transfer in the developing region of the channel, but this is reversed based on using x^*.

Acknowledgments—The financial support of Isfahan University of Technology in Islamic Republic of Iran, to one of the authors (S. Gh. Etemad) is gratefully acknowledged. Also, the authors acknowledge the Computer Center of McGill University for the major grant to use the mainframe facilities and the National Sciences and Engineering Research Council (NSERC) and Exergex corporation for partial support of this research.

REFERENCES

1. R. K. Shah and A. L. London, Laminar flow forced convection in ducts. In *Advances in Heat Transfer* (Edited by T. F. Irvine Jr and J. P. Hartnett). Academic Press, New York (1978).
2. R. K. Shah and M. S. Bhatti, Laminar convection heat transfer in ducts. In *Handbook of Single-Phase Convective Heat Transfer* (Edited by S. Kakac, R. K. Shah and W. Aung), Chap. 3, no. 3.1–3.137. Wiley, New York (1987).
3. E. R. G. Eckert, T. F. Irvine Jr and J. T. Yen, Local laminar heat transfer in wedge-shaped passages, *Trans. ASME* **80,** 1433–1438 (1958).
4. E. M. Sparrow and A. Haji-Sheikh, Laminar heat transfer and pressure drop in isosceles triangular, right triangular and circular sector ducts, *J. Heat Transfer* **87,** 426–427 (1965).
5. M. H. Hu, Flow and thermal analysis for mechanically enhanced heat transfer tubes. Ph.D. Thesis, Department of mechanical engineering, State University of New York at Buffalo (1973).
6. M. H. Hu and Y. P. Chang, Optimization of finned tubes for heat transfer in laminar flow, *Trans. ASME* **95,** 332–338 (1973).
7. H. M. Soliman, A. A. Munis and A. C. Trupp, Laminar flow in the entrance region of circular sector ducts, *Trans. ASME* **49,** 640–642 (1982).
8. Q. M. Lei and A. C. Trupp, Maximum velocity location and pressure drop of fully developed laminar flow in circular sector ducts, *Trans. ASME* **111,** 1085–1087 (1989).
9. Q. M. Lei and A. C. Trupp, Further analysis of laminar heat transfer in circular sector ducts, *Trans. ASME* **111,** 1088–1090 (1989).
10. A. C. Trupp and Q. M. Lei, Laminar flow heat transfer in circular sector ducts with uniform heat flux, *Trans. CSME* **13,** 31–34 (1989).
11. A. C. Trupp and A. C. Y. Lau, Fully developed laminar heat transfer in circular sector ducts with isothermal walls, *J. Heat Transfer* **106,** 467–469 (1984).
12. T. M. Ben-Ali, H. M. Soliman and E. K. Zariffeh, Further results for laminar heat transfer in annular sector and circular sector ducts, *Trans. ASME* **111,** 1090–1093 (1989).
13. S. W. Hong and A. E. Bergles, Laminar flow heat transfer in the entrance region of semi-circular tubes with uniform heat flux, *Int. J. Heat Mass Transfer* **19,** 123–124 (1976).
14. R. M. Manglik and A. E. Bergles, Laminar flow heat transfer in a semi-circular tube with uniform wall temperature, *Int. J. Heat Mass Transfer* **31,** 625–636 (1988).
15. Q. M. Lei and A. C. Trupp, Forced convection of thermally developing laminar flow in circular sector ducts, *Int. J. Heat Mass Transfer* **33,** 1675–1683 (1990).
16. C. Prakash and Ye-Di Liu, Analysis of laminar flow and heat transfer in the entrance region of an internally finned circular duct, *Trans. ASME* **107,** 84–91 (1985).
17. R. P. Hsia and B. T. F. Chung, Fluid flow and heat transfer for power-law fluids in annular sector ducts with constant wall temperature circumferentially, *National Heat Transfer Conf. ASME* **93-HT-11,** 1–9 (1993).
18. J. K. Dasmahapatra and R. P. Hsia, Laminar flow heat transfer to generalized power law fluids inside circular tubes fitted with regularly spaced twisted tape elements for uniform wall temperature condition, *Fund. Heat Transfer non-Newt. Fluids* **HTD-174,** 51–58 (1991).
19. A. Lawal and A. S. Mujumdar, Laminar duct flow and heat transfer to purely viscous non-Newtonian fluids. In *Advances in transport processes* (Edited by A. S. Mujumdar and R. A. Mashelkar). pp. 352–443. Wiley Interscience, New York (1989).
20. S. Gh. Etemad, A. S. Mujumdar and B. Huang, Viscous dissipation effects in entrance region heat transfer for a power law fluid flowing between parallel plates, *Int. J. Heat Fluid Flow* **15,** 122–131 (1994).
21. S. Gh. Etemad, A. S. Mujumdar and B. Huang, Laminar forced convection heat transfer of a non-Newtonian fluid in the entrance region of a square duct with different boundary conditions, *Proc. 10th Int. Heat Transfer Conf.*, Vol. 4, pp. 231–236. Taylor & Francis, New York (1994).
22. O. C. Zienkiewicz, *Finite Element Method.* McGraw-Hill, New York (1977).
23. J. F. Pittman, Finite Elements for Field Problems, *Fundamentals of Computer Modeling for Polymer Processing* (Edited by Ch. L. Tucker III). Hanser, New York (1989).
24. M. S. Engleman, FIDAP theoretical manual revision 6. Fluid Dynamics International Inc., 500 Davis St, Suite 600, Evanston, IL (1991).